ARCHIVES OF ELECTRICAL ENGINEERING VOL. 67(3), pp. 579–589 (2018)

DOI 10.24425/123664

Design and analysis of the ferrite air-gapped cores for a resonant inductor

JIANFEN ZHENG, CHUNFANG WANG, DONGWEI XIA

College of Automation Engineering, Qingdao University
Qingdao 266071, China
e-mail: {jianfenzh/XDW}@qdu.edu.cn, qduwcf@163.com

(Received: 02.03.2018, revised: 03.06.2018)

Abstract: In this paper, a three-air-gapped structure of a ferrite core for a resonant inductor is proposed. The electromagnetic and thermal field models are built using a 3D finite element method. Compared with the conventional signal-air-gapped structure of a ferrite core, the simulation and analysis results show that the proposed three-air-gapped ferrite core resonant inductor can reduce eddy-current loss and decrease temperature rise. In addition, the optimal position of air-gapped is presented.

Key words: three-air-gapped, electromagnetic and thermal field, finite element method, resonant inductor

1. Introduction

In recent years, an inductance-inductance-capacitance (LLC) resonant converter is very attractive topology for high-power applications because of its attractive features: smooth waveforms, high efficiency and high power density [1–4]. In the resonant inductors of the LLC converter, the current waveform includes the higher order harmonic components caused by switching. For this reason, excellent high frequency magnetic properties are necessary in iron core materials for use in high frequency inductors. Soft ferrites demonstrate properties such as low power loss and high permeability, which make them very useful and appropriate for use in power electric applications [5, 6]. The core loss evaluation was performed, and the influence of inductor gaps on iron loss was proposed in [7–9]. A simplified 2D model was presented to investigate influence of an air-gap in the magnetic field as describe in [10]. A 3D magnetic field is analyzed related to the solution of Laplace's and Poisson's equations by the finite element method [11]. In [12], a dynamic, nonlinear magnetic field analysis of a reactor core with air-gap was carried out.

However, these studies, based on the finite element analysis, are directed at the study of the ferrite core, taking into account the single air-gapped core only. Eddy currents are induced in the air-gapped ferrite core due to fringing flux, and this causes local overheating. In order to reduce the eddy-current loss and decrease temperature rise, a three-air-gapped structure of a ferrite core

for a resonant inductor is proposed in this paper. The resonant inductor of the LLC resonant converter is shown in Fig. 1, which is applied in the battery-pile circuit of an electric car.

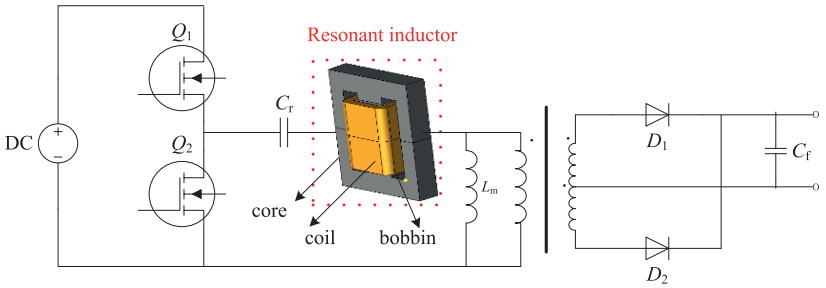

Fig. 1. Topology circuit of LLC resonant convertor

The electromagnetic and thermal field coupled model is built using a 3D finite element method (FEM). Compared with the conventional single-air-gapped ferrite core, the simulated results indicate that the proposed three-air-gapped ferrite core can reduce eddy-current loss and decrease temperature rise. In addition, it is presented for a three-air-gapped optimal curve and the optimum placement.

2. Proposed structure of ferrite core inductor

Fig. 2 shows the model inductor used for simulation and analysis.

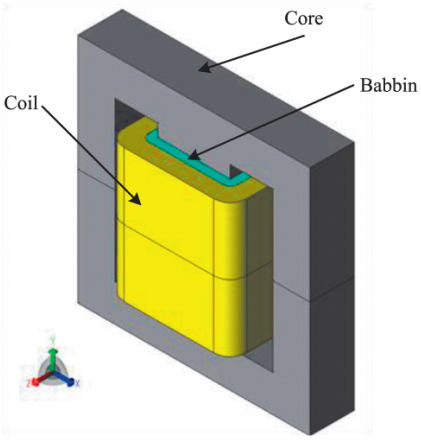

Fig. 2. Resonant inductor of LLC resonant convertor

A dual-E magnetic core with a single-air-gap is generally used as magnetic core of a resonant inductor. The single-air-gapped ferrite core structure is shown in Fig. 3(a). As it is known to all, eddy currents are induced in a magnetic core due to the leakage of magnetic flux, which can cause local overheating. In order to reduce local eddy current loss and avoid local heating, a three-air-gapped structure of a ferrite core is proposed, as shown in Fig. 3(b).

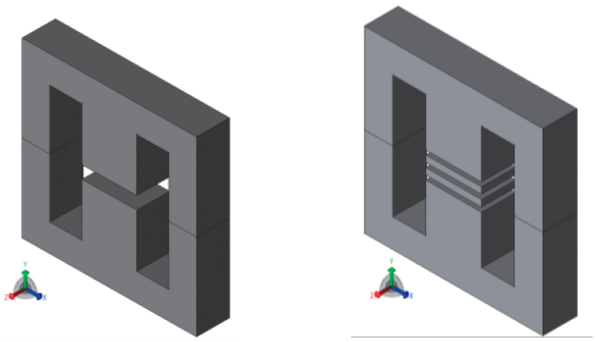

(a) (b)

Fig. 3. Ferrite core structure of resonant inductor: (a) single-air-gapped; (b) three-air-gapped

In the linear region, the air-gapped thickness has considerable influence on the inductance value. As the thickness increase, the inductance values intensity increases too [13]. In this paper, the inductance value will be unchanged. The total air-gapped thickness is equal to 4 mm, and the air-gapped is evenly divided into three parts. The main dimensions of the ferrite core are presented in Fig. 4.

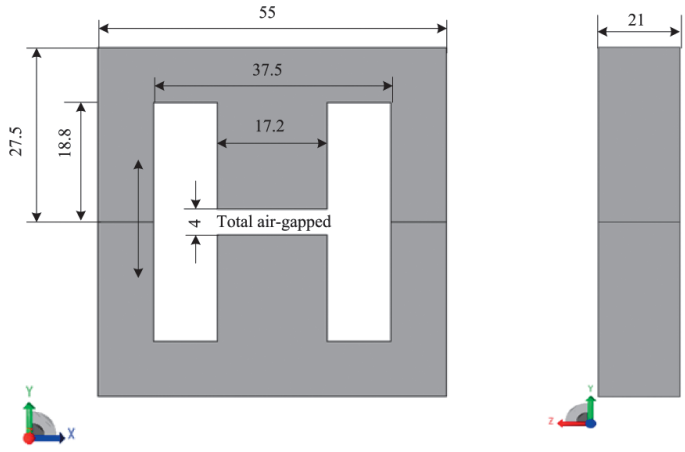

Fig. 4. Main dimensions of ferrit core for resonant inductor

3. Mathematical models of resonant inductor

To calculate the core loss and temperature distribution, FEM has been used. Due to the symmetry of the object, only the halved cross has been considered. The total loss of the resonant inductor, Q, consists of the ferrite core loss, Q_{core}, and the conduction loss, Q_{Cu}, of the joules

www.czasopisma.pan.pl PAN POLSKA AKADEMIA NAUK www.journals.pan.pl

loss in the coils. Moreover, Q_{core} can be divided into the material loss, Q_{mat}, derived from the main flux density flowing in the rolling direction and transverse direction, and the eddy current loss, Q_{eddy}, due to leakage magnetic flux flowing vertical to laminating direction [14]. Therefore, Q can be defined as:

$$Q = Q_{\text{core}} + Q_{\text{Cu}} = Q_{\text{mat}} + Q_{\text{eddy}} + Q_{\text{Cu}} \,. \tag{1}$$

3.1. Electromagnetics fields calculation

The material loss Q_{mat} is obtained from the following Steinmetz's equation made by datasheet (EE55/28/21):

$$Q_{\text{mat}} = \sum_{i=1}^{n} \left(K_h B_{(i)}^2 f + K_e B_{(i)}^2 f^2 \right) V(i) \,, \tag{2}$$

where K_h and K_e are the coefficients calculated from the datasheet, B is the magnetic flux density, f is the frequency, V is the volume, and n is the number of elements, it means the element number. The material loss is caused by main flux density, B, from the rolling direction and the transverse direction.

The eddy current loss by the leakage magnetic flux is calculated with the Elektra-SS modulus of the Opera-3D package [15]. In the paper, the $\boldsymbol{A}$-V-$\boldsymbol{A}$ method is adopted in a 3D eddy current analysis model for FEM. In the region where the eddy currents arise, the equation for the total vector potential $\boldsymbol{A}$ and an electric scalar potential V has to be solved as the following:

$$\nabla \times \frac{1}{\mu} \nabla \times \boldsymbol{A} - \nabla \frac{1}{\mu} \nabla \times \boldsymbol{A} + \sigma \frac{\partial \boldsymbol{A}}{\partial t} + \sigma \nabla V = 0 \,, \tag{3}$$

where σ is the electrical conductivity, and μ is the magnetic permeability of the material.

According to Equation (3), the eddy current loss Q_{eddy} is achieved as the following:

$$Q_{\text{eddy}} = \frac{1}{\sigma} |\boldsymbol{J}|^2 = \frac{1}{\sigma} \left| \nabla \times \frac{1}{\mu} \nabla \times \boldsymbol{A} \right|^2 , \tag{4}$$

where J is the current density.

The joules loss in the coils is taken into account as the following:

$$Q_{\text{Cu}} = \sum_{j=1}^{k} I_{(j)}^2 R_{(j)} \,, \tag{5}$$

where $I_{(j)}$ is the $j^{\text{-th}}$ coil current, $R_{(j)}$ is the $j^{\text{-th}}$ coil resistance. $R_{(j)}$ can be written as follows:

$$R_{(j)} = \rho \frac{l_{(j)}}{S_{(j)}} = \frac{\rho n_{(j)} (MLT)}{A_W K_u \alpha_{(j)} / n_{(j)}} = \frac{\rho n_{(j)}^2 (MLT)}{A_W K_u \alpha_{(j)}} \,, \tag{6}$$

where ρ is the coil density, $l_{(j)}$ is the $j^{-\text{th}}$ coil length, $S_{(j)}$ is the $j^{-\text{th}}$ coil area, $n_{(j)}$ is the turn number, MLT is mean the length per turn, A_W is the core windows area, $\alpha_{(j)}$ is the fraction of the $j^{-\text{th}}$ coil windows area, and K_u is the winding fill factor.

www.czasopisma.pan.pl PAN POLSKA AKADEMIA NAUK www.journals.pan.pl

According to Equation (5) and (6), the joules loss in the coils can be defined as follows:

$$Q_{\mathrm{Cu}} = \frac{\rho(MLT)}{A_W K_u} \sum_{j=1}^{k} \frac{I_{(j)}^2 n_{(j)}^2}{\alpha_{(j)}} . \tag{7}$$

The joules loss is optimal provided as follows [15]:

$$Q_{\mathrm{Cu}} = \frac{\rho(MLT)}{A_W K_u} \sum_{j=1}^{k} \frac{I_{(j)} n_{(j)}}{\alpha_{(j)}} . \tag{8}$$

3.2. Thermal fields calcaulation

The heating phenomenon depends on thermal conductivity λ, thermal capacitance c, mass density ρ, feed thermal power density Q, and the thermal power exchange between the object and surrounding. The material propriety parameters are shown in Table 1. For calculation the temperature T, a heat conduction equation is given in the thermal field as the following [16]:

$$\nabla \cdot (\lambda \nabla T) + Q = \rho c \frac{\partial T}{\partial t} . \tag{9}$$

Table 1. Material properties used in thermal model

Property	Ferrite	Copper	Bobbin	Air
Thermal conductivity λ [W/(m·K)]	5	401	0.22	0.031
Thermal capacitance c [J/(kg·K)]	750	386	1000	1007
Mass density ρ [kg/m^3]	4850	8930	1600	1.205

In the temperature field analysis, boundary conditions should be imposed. Outer surface is a vertical square surface and can be assumed as a vertical plate. Two types of heat transfer can occur in the outer surface, including radiation and natural convection. On the calculation region boundaries, $T_0 = 25°\mathrm{C}$ has been forced as Dirichlet's condition. The heat transfer boundary condition on the surface of the inductor is given as the following:

$$\lambda(\boldsymbol{n} \cdot \nabla T) + h(T - T_0) = 0, \tag{10}$$

where $\boldsymbol{n}$ is the normal vector outside of the border, h is the heat transfer coefficient, and T_0 is the ambient temperature.

Thermal radiation phenomenon is not included in the Tempo solver. Thus, we have modified the boundary condition coefficient taking into account the radiation coefficient in the heating process, according to the following equation [17].

$$h_{\mathrm{eq}} = h + 4\sigma_B \varepsilon \left((T + T_0)/2\right)^3 , \tag{11}$$

where σ_B is the Stefan-Boltzmann constant and $\varepsilon = 0.9$ is the emittance value.

In order to calculate electromagnetic and thermal fields, a suggested flow chart is shown in Fig. 5. Firstly, some electromagnetic data are input such as material properties, ambient temperature, simulation time and step size. According to eddy current region control, the electromagnetic

www.czasopisma.pan.pl PAN POLSKA AKADEMIA NAUK www.journals.pan.pl

calculation and analysis are carried on. Secondly, the eddy current loss and the joules loss are used as the heat generating source load of the thermal field. The calculation and analysis of the thermal field are carried out for the inductor surface and internal temperature. Then, determine whether the set time is up to the simulation end time. If not met, update parameters of the material properties according to the calculated temperature. While you increase the simulation time step, calculate the electromagnetic field again, and repeat the process until the end time. When the simulation is done, the results are saved and transferred to the treatment store so as to be read, viewed and ready for other operation.

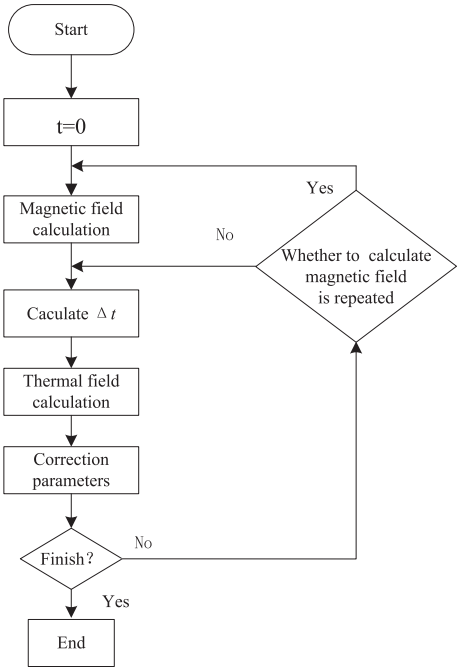

Fig. 5. Flow chart to coupling field calculation

4. Results Analysis and Air-gapped Optimization Discussion

In the paper, the calculations and measurements have been carried out for both a single-air-gapped and three-air-gapped ferrite core of the considered inductor. In the case of both analyzed models, the maximal values of the magnetic flux density inside the core is equal to $B_m = 0.3$ T. The supply frequency of the sinusoidal current wave is $f = 10$ kHz, and the current RMS is equal to $I = 13$ A. The electromagnetic and thermal fields are calculated and analyzed for the resonant inductor using FEM.

4.1. Electromagnetic fields analysis

Fig. 6 shows the distribution of magnetic flux density B in the resonant inductor core at the time of maximum coil current.

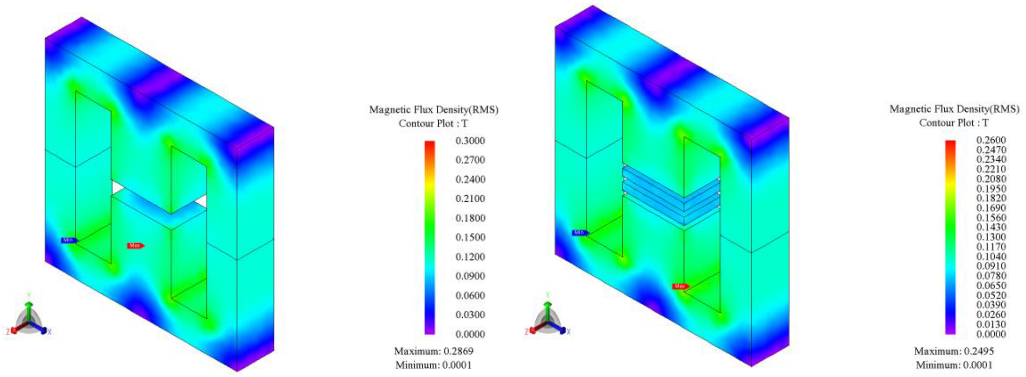

(a) (b)

Fig. 6. Magnetic flux density of resonant inductor ferrite core: (a) single-air-gapped core; (b) three-air-gapped core

In the single-air-gapped core model shown in Fig. 6(a), it can be observed that there are large magnetic flux densities compared with the three-air-gapped model shown in Fig. 6(b). The leakage magnetic flux cannot enter into the ferrite core, because of having permeability on the Y-direction. The magnetic flux concentrates on the surface of the core. On the other hand, the magnetic flux densities near the gap are distributed uniformly on the three-air-gapped model because the leakage magnetic flux densities are small. Eddy current is induced in the ferrite core due to leakage magnetic flux. Therefore, the proposed three-air-gapped core structure can reduce eddy current loss.

Fig. 7 shows the distribution of ferrite core loss Q. From the simulation, it can be obtained that the maximum loss density is $Q = 3425600$ W/m^3 in a single-air-gapped core as shown in Fig. 7(a). By contrast, the maximum loss density is $Q = 2558800$ W/m^3 in three-air-gapped core as shown

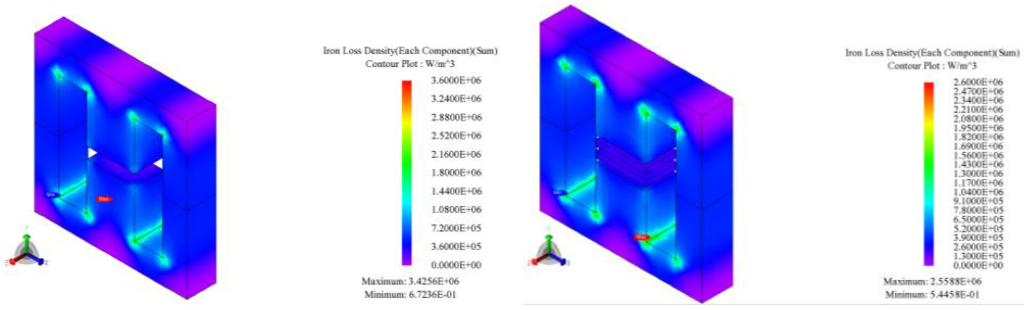

(a) (b)

Fig. 7. Ferrite core loss of resonant inductor ferrite core: (a) single-air-gapped core; (b) three-air-gapped core

in Fig. 7(b). As a conclusion, in this section, it is revealed that the proposed three-air-gapped structure can reduce ferrite core loss.

4.2. Thermal fields analysis

The obtained loss distribution has been assumed for the thermal model. In this simulation, it is assumed that the heat transfer between the coil and core of the inductor has been naturally done. The film coefficient is considered equal to 10 W/m^2°C.

Fig. 8 shows the static thermal field distribution in the resonant inductor, and Fig. 9 shows the static thermal field distribution in the ferrite core of the resonant inductor. From the simulation, it can be seen that the higher temperature is distributed in the ferrite core. The maximum temperature value of the single-air-gapped core inductor reaches 65°C, whereas for the three-air-gapped core inductor, the maximum temperature value is equal to 53°C. By contrast, the proposed three-air-

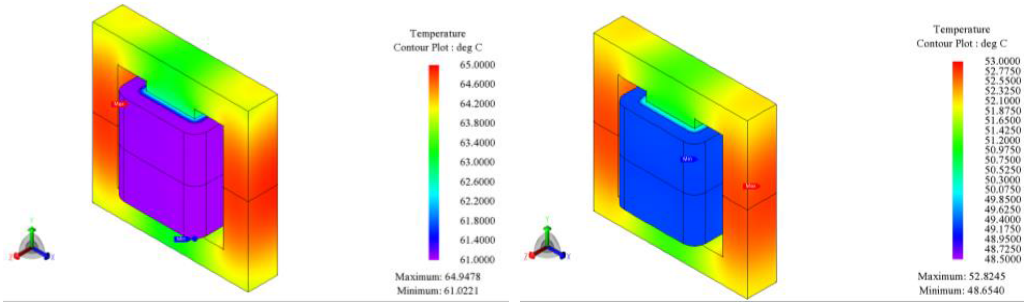

(a) (b)

Fig. 8. Temperature distribution of resonent inductor: (a) single-air-gapped core; (b) three-air-gapped core

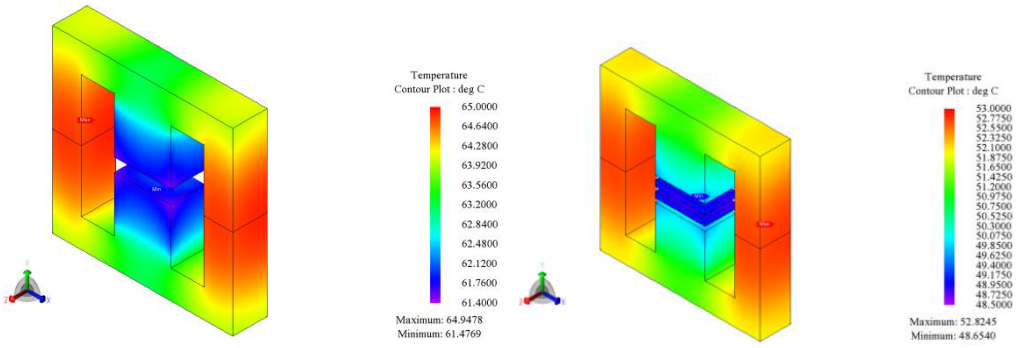

(a) (b)

Fig. 9. Temperature distribution of resonent inductor ferrite core: (a) single-air-gapped core; (b) three-air-gapped core

gapped core can decrease temperature by more than 10 degree. Therefore the three-air-gapped structure is adopted to decrease temperature rise.

4.3. Air-gap position discussion

In this paper, the air-gap position is discussed. Because the total thickness of air-gap is unchanged and its value is 4mm, the selection of the air-gap position depends on the thickness of ferrite core block S as shown in Fig. 10.

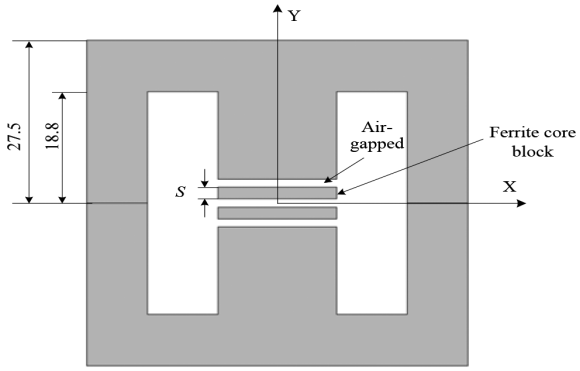

Fig. 10. Cross-section of three-air-gapped ferrite core

In order to find the air-gap position that leads to the lowest temperature rise, many simulation and calculation have been carried out. The maximum temperature curve for the length of a magnetic core block is presented as shown in Fig. 11.

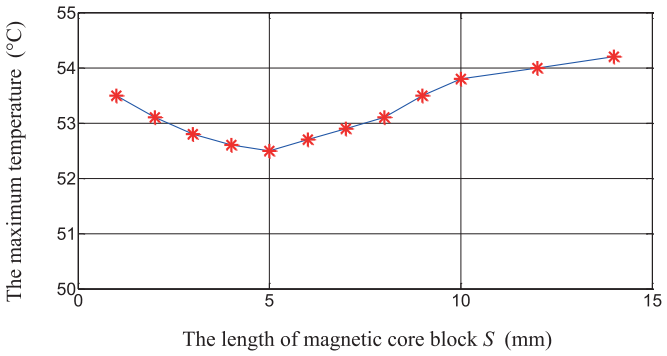

Fig. 11. The maximum temperature curve for the length of magnetic core block

From Fig. 11, it can be seen that when the length value of the magnetic core block is 5 mm, the maximum temperature of the ferrite core is 52.5°C, that is the lowest temperature rise. As a conclusion, it is revealed that the optimal positions of three air-gaps are respectively (−7.00, −5.67), (−0.67, 0.67), (5.67, 7.00) on the Y-direction.

www.czasopisma.pan.pl PAN POLSKA AKADEMIA NAUK www.journals.pan.pl

5. Conclusion

In this paper, a modeling procedure and the design criterion for the simulation in a 3D of a ferrite air-gapped core for a resonant inductor have been proposed. The electromagnetic field and thermal field of the resonant inductor have been calculated and analyzed. The simulation reveals that the three-air-gapped core can reduce eddy current loss and can decrease temperature rise compared with a single-air-gapped core. Furthermore, the maximum temperature curve for the length of a magnetic core block is presented, and it reveals the optimal positions of its three air-gaps.

References

[1] Wu W., Huang M., Blaabjerg F., *Efficiency comparison between the LLCLand LCL-filters based single-phase grid-tied inverters*, Archives of Electrical Engineering, vol. 63, no. 1, pp. 63–79 (2014).

[2] Kundu U., Yenduri K., Sensarma P., *Accurate ZVS Analysis for Magnetic Design and Efficiency Improvement of Full-Bridge LLC Resonant Converter*, IEEE Transactions on Power Electronics, vol. 32, no. 3, pp. 1703–1706 (2017).

[3] Zong S., Luo H., Li W., *Theoretical Evaluation of Stability Improvement Brought by Resonant Current Loop for Paralleled LLC Converters*, IEEE Transactions on Industrial Electronics, vol. 62, no. 7, pp. 4170–4180 (2015).

[4] Seeman M.D., *GaN Devices in Resonant LLC Converters: System-level considerations*, IEEE Power Electronics Magazine, vol. 2, no. 1, pp. 36–41 (2015).

[5] Macrelli E., Romani A. *et al.*, *Modeling, Design, and Fabrication of High-Inductance Bond Wire Microtransformers With Toroidal Ferrite Core*, IEEE Transactions on Power Electronics, vol. 30, no. 10, pp. 5724–5737 (2015).

[6] Salas R.A., Pleite J., *Equivalent Electrical Model of a Ferrite Core Inductor Excited by a Square Waveform Including Saturation and Power Losses for Circuit Simulation*, IEEE Transactions on magnetics, vol. 49, no. 7, pp. 4257–4260 (2013).

[7] Ahour J.N., Seyedtabah A., Gharehpetian G.B., *On the accuracy of detailed model inductance matrix estimation for air core winding*, Archives of Electrical Engineering, vol. 66, no. 4, pp. 787–799 (2017).

[8] Hilal A., Raulet M.A., Martin C., Sixdenier F., *Power Loss Prediction and Precise Modeling of Magnetic Powder Components in DC–DC Power Converter Application*, IEEE Transactions on Power Electronics, vol. 30, no. 4, pp. 2232–2238 (2015).

[9] Gao Y. *et al.*, *Loss reduction of reactor with grain-oriented silicon steel plates*, IEEE Transaction on Magnetics, vol. 49, no. 5, pp. 1973–1976 (2013).

[10] Salas R.A., Pleite J., *Simulation of the Saturation and Air-Gap Effects in a POT Ferrite Core With a 2-D Finite Element Model*, IEEE Transactions on Magnetics, vol. 47, no. 10, pp. 4135–4138 (2011).

[11] Kurita N., Onda K., Nakanoue K., Inagaki K., *Loss estimation method for three-phase AC reactors of two types of structures using amorphous wound cores in 400-kVA UPS*, IEEE Transactions on Power Electronics, vol. 29, no. 7, pp. 3657–3688 (2014).

[12] Tomczuk B., Babczyk K., *Calculation of the self- and mutual inductances and 3-D magnetic fields of chokes with air gaps in core*, Electrical Engineering (Archiv fur Elektrotechnik), Springer-Verlag, Berlin, vol. 83, pp. 41–46 (2001).

[13] Macrelli E. *et al.*, *Modeling, Design, and Fabrication of High-Inductance Bond Wire Microtransformers With Toroidal Ferrite Core*, IEEE Transactions on Power Electronics, vol. 30, no. 10, pp. 5724–5737 (2015).

www.czasopisma.pan.pl PAN POLSKA AKADEMIA NAUK www.journals.pan.pl

[14] Tsili M.A., Amoiralis E.I., Kladas A.G., Souflaris A.T., *Power transformer thermal analysis by using an advanced coupled 3D heat transfer and fluid flow FEM model*, International Journal of Thermal Sciences, vol. 53, pp. 188–201 (2012).

[15] Zhiguang C., Takahashi N., Forghani B. *et al.*, *Electromagnetic and Thermal Field Modeling and Application in Electrical Engineering*, Science China Press (2009).

[16] Hayt W.H., Buck J.A., *Engineering Electromagnetics*, 7th Edition, the McGraw-Hill Companies, Inc. (2006).

[17] Tomczuk B.Z. *et al.*, *Electromagnetic and temperature 3-D fields for the modular transformers heating under high-frequency operation*, IEEE Trans. Magn., vol. 50, no. 2 (2014).